

Wide wavelength selectable all-fiber thulium doped fiber laser between 1925 nm and 2200 nm

Jianfeng Li,^{1,2,*} Zhongyuan Sun,¹ Hongyu Luo,² Zhijun Yan,¹ Kaiming Zhou,¹
Yong Liu,² and Lin Zhang¹

¹Aston Institute of Photonic Technologies (AIPT), Aston University, Birmingham, UK

²State Key Laboratory of Electronic Thin Films and Integrated Devices, School of Optoelectronic Information, University of Electronic Science and Technology of China (UESTC), Chengdu 610054, China

*lijianfeng@uestc.edu.cn

Abstract: We demonstrate an all-fiber Tm³⁺-doped silica fiber laser operating at a wide selectable wavelength range by using different fiber Bragg gratings (FBGs) as wavelength selection elements. With a specifically designed high reflective (HR) FBG and the fiber end as an output coupler, the lasing in the range from 1975 nm to 2150 nm with slope efficiency of >30% can be achieved. By employing a low reflective (LR) FBG as the output coupler, the obtainable wavelengths were extended to the range between 1925 nm and 2200 nm which is the reported longest wavelength from the Tm³⁺-doped silica fiber lasers. Furthermore, by employing a FBG array in the laser cavity and inducing bend loss between adjacent FBGs in the array, six switchable lasing wavelengths were achieved.

©2014 Optical Society of America

OCIS codes: (140.3510) Lasers, fiber; (140.3480) Lasers, diode-pumped.

References and links

1. S. W. Henderson, C. P. Hale, J. R. Magee, M. J. Kavaya, and A. V. Huffaker, "Eye-safe coherent laser radar system at 2.1 μm using Tm:Ho:YAG lasers," *Opt. Lett.* **16**(10), 773–775 (1991).
2. N. Sugimoto, N. Sims, K. Chan, and D. K. Killinger, "Eye-safe 2.1- μm Ho lidar for measuring atmospheric density profiles," *Opt. Lett.* **15**(6), 302–304 (1990).
3. D. E. Johnson, "Use of the holmium:YAG (Ho:YAG) laser for treatment of superficial bladder carcinoma," *Lasers Surg. Med.* **14**(3), 213–218 (1994).
4. A. Leunig, P. Janda, R. Sroka, R. Baumgartner, and G. Grevers, "Ho:YAG laser treatment of hyperplastic inferior nasal turbinates," *Laryngoscope* **109**(10), 1690–1695 (1999).
5. S. Futao, Z. Wentong, Z. Yan, D. Qingyu, and L. Aiwu, "Application of endoscopic Ho:YAG laser incision technique treating urethral strictures and urethral atresias in pediatric patients," *Pediatr. Surg. Int.* **22**(6), 514–518 (2006).
6. S. D. Jackson and T. A. King, "High-power diode-cladding-pumped Tm-doped silica fiber laser," *Opt. Lett.* **23**(18), 1462–1464 (1998).
7. K. Oh, T. F. Morse, A. Kilian, L. Reinhart, and P. M. Weber, "Continuous-wave oscillation of thulium-sensitized holmium-doped silica fiber laser," *Opt. Lett.* **19**(4), 278–280 (1994).
8. S. D. Jackson, A. Sabella, A. Hemming, S. Bennetts, and D. G. Lancaster, "High-power 83 W holmium-doped silica fiber laser operating with high beam quality," *Opt. Lett.* **32**(3), 241–243 (2007).
9. S. D. Jackson, "8.8 W diode-cladding-pumped Tm³⁺, Ho³⁺-doped fluoride fibre laser," *Electron. Lett.* **37**(13), 821–822 (2001).
10. B. M. Walsh and N. P. Barnes, "Comparison of Tm: ZBLAN and Tm: silica fiber lasers; Spectroscopy and tunable pulsed laser operation around 1.9 μm ," *Appl. Phys. B* **78**(3-4), 325–333 (2004).
11. R. Li, J. Li, L. Shterengas, and S. D. Jackson, "Highly efficient holmium fiber laser diode pumped at 1.94 μm ," *Electron. Lett.* **47**(19), 1089–1090 (2011).
12. Y. H. Tsang, T. A. King, D. K. Ko, and J. M. Lee, "Broadband amplified spontaneous emission double-clad fiber source with central wavelengths near 2 μm ," *J. Mod. Opt.* **53**(7), 991–1001 (2006).
13. D. Y. Shen, L. Pearson, P. Wang, J. K. Sahu, and W. A. Clarkson, "Broadband Tm-doped superfluorescent fiber source with 11 W single-ended output power," *Opt. Express* **16**(15), 11021–11026 (2008).
14. J. Liu and P. Wang, "High-power broadband thulium-doped all-fiber superfluorescent source at 2 μm ," *IEEE Photonics Technol. Lett.* **25**(3), 242–245 (2013).
15. W. A. Clarkson, N. P. Barnes, P. W. Turner, J. Nilsson, and D. C. Hanna, "High-power cladding-pumped Tm-doped silica fiber laser with wavelength tuning from 1860 to 2090 nm," *Opt. Lett.* **27**(22), 1989–1991 (2002).
16. C. Guo, D. Shen, J. Long, and F. Wang, "High-power and widely tunable Tm-doped fiber laser at 2 μm ," *Chin. Opt. Lett.* **10**(9), 091406 (2012).

17. Z. Li, S. U. Alam, Y. Jung, A. M. Heidt, and D. J. Richardson, "All-fiber, ultra-wideband tunable laser at 2 μm ," *Opt. Lett.* **38**(22), 4739–4742 (2013).
18. M. Tokurakawa, J. M. O. Daniel, S. Chenug, H. Liang, and W. A. Clarkson, "Ultra-broadband wavelength swept Tm-Doped fiber laser," in *CLEO Europe-IQEC* (2013), pp. 12–16.
19. Z. S. Sacks, Z. Schiffer, and D. David, "Long wavelength operation of double-clad Tm: silica fiber lasers," *Proc. SPIE* **6453**, 645320 (2007).
20. S. D. Jackson, F. Bugge, and G. Erbert, "High-power and highly efficient diode-cladding-pumped Ho³⁺-doped silica fiber lasers," *Opt. Lett.* **32**(22), 3349–3351 (2007).
21. A. Hemming, S. D. Jackson, A. Sabella, S. Bennetts, and D. G. Lancaster, "High power, narrow bandwidth and broadly tunable Tm³⁺, Ho³⁺-co-doped aluminosilicate glass fiber laser," *Electron. Lett.* **46**(24), 1617–1618 (2010).
22. N. Simakov, A. Hemming, W. A. Clarkson, J. Haub, and A. Carter, "A cladding-pumped, tunable holmium doped fiber laser," *Opt. Express* **21**(23), 28415–28422 (2013).
23. S. O. Antipov, V. A. Kamynin, O. I. Medvedkov, A. V. Marakulin, L. A. Minashina, A. S. Kurkov, and A. V. Baranikov, "Holmium fiber laser emitting at 2.21 μm ," *Quantum Electron.* **43**(7), 603–604 (2013).
24. R. M. Percival, S. F. Carter, D. Szebesta, S. T. Davey, and W. A. Stallard, "Thulium-doped monomode fluoride fiber laser broadly tunable from 2.25 to 2.5 μm ," *Electron. Lett.* **27**(21), 1912–1913 (1991).
25. R. Allen and L. Esterowitz, "CW diode pumped 2.3 μm fiber laser," *Appl. Phys. Lett.* **55**(8), 721–722 (1989).
26. R. G. Smart, J. N. Carter, A. C. Tropper, and D. C. Hanna, "Continuous-wave oscillation of Tm³⁺-doped fluorozirconate fibre lasers at around 1.47 μm , 1.9 μm and 2.3 μm when pumped at 790 nm," *Opt. Commun.* **82**(5–6), 563–570 (1991).
27. R. M. El-Agmy and N. M. Al-Hosiny, "2.31 μm laser under up-conversion pumping at 1.064 μm in Tm³⁺: ZBLAN fiber lasers," *Electron. Lett.* **46**, 936–937 (2010).
28. T. Sumiyoshi, H. Sekita, T. Arai, S. Sato, M. Ishihara, and M. Kikuchi, "High-power continuous-wave 3- and 2- μm cascade Ho³⁺: ZBLAN fiber laser and its medical applications," *IEEE J. Sel. Top. Quantum Electron.* **5**(4), 936–943 (1999).
29. A. Guhur and S. D. Jackson, "Efficient holmium-doped fluoride fiber laser emitting 2.1 μm and blue upconversion fluorescence upon excitation at 2 μm ," *Opt. Express* **18**(19), 20164–20169 (2010).
30. J. L. Yang, S. C. Tjin, and N. Q. Ngo, "A novel wavelength switchable fiber laser source and its application in photonics beamforming for optically controlled phased array antenna," *Appl. Phys. B* **78**(3–4), 345–349 (2004).
31. G. Souhaite, R. Delepine, O. Pellegrini, E. Vassilakis, M. Stellmacher, P. Graindorge, and P. Martin, "16 channels, switchable external cavity-based multi-wavelength laser for DWDM applications," in *Proc. 27th ECOC 2* (2001), pp. 196–197.
32. S. Tanaka, H. Yokosuka, T. Ogawa, and N. Takahashi, "Wavelength-switchable fiber laser for thermally stabilized fiber Bragg grating vibration sensor array," in *Proc. IEEE Sensors* (2004), pp. 1301–1304.
33. Q. H. Mao and J. W. Y. Lit, "Switchable multiwavelength erbium-doped fiber laser with cascaded fiber grating cavities," *IEEE Photonics Technol. Lett.* **14**(5), 612–614 (2002).
34. C. L. Zhao, X. F. Yang, C. Lu, N. J. Hong, X. Guo, P. R. Chaudhuri, and X. Y. Dong, "Switchable multi-wavelength erbium-doped fiber lasers by using cascaded fiber Bragg gratings written in high birefringence fiber," *IEEE Photonics Technol. Lett.* **230**, 313–317 (2004).
35. J. A. Alvarez-Chavez, A. Martínez-Rios, I. Torres-Gomez, and H. L. Offerhaus, "Wide wavelength-tuning of a double-clad Yb³⁺-doped fiber laser based on a fiber Bragg grating array," *Laser Phys. Lett.* **4**(12), 880–883 (2007).
36. I. Torres-Gomez, A. Martínez-Rios, G. Anzueto-Sanchez, R. Selvas-Aguilar, A. Martínez-Gomez, and D. Monzon-Hernandez, "Multi-wavelength-switchable double clad Yb³⁺-doped fiber laser based on reflectivity control of fiber Bragg gratings by induced bend loss," *Opt. Rev.* **12**, 65–68 (2005).
37. W. J. Peng, F. P. Yan, Q. Li, S. Liu, T. Feng, S. Y. Tan, and S. C. Feng, "1.94 μm switchable dual-wavelength Tm³⁺ fiber laser employing high-birefringence fiber Bragg grating," *Appl. Opt.* **52**(19), 4601–4607 (2013).
38. H. M. Pask, R. J. Carman, D. C. Hanna, A. C. Tropper, C. J. Mackechnie, P. R. Barber, and J. M. Dawes, "Ytterbium-doped silica fiber lasers: versatile sources for the 1-1.2 μm region," *IEEE J. Sel. Top. Quantum Electron.* **1**(1), 2–13 (1995).
39. Y. Kimura and M. Nakazawa, "Lasing characteristics of Er³⁺-doped silica fibers from 1553 up to 1603 nm," *J. Appl. Phys.* **64**(2), 516–520 (1988).
40. M. R. A. Moghaddam, S. W. Harun, and H. Ahmad, "Comparison between analytical solution and experimental setup of a short long ytterbium doped fiber laser," *Opt. Photonics J.* **2**(2), 65–72 (2012).
41. E. Desurvire, "Analysis of gain difference between forward-and backward-pumped erbium-doped fiber amplifiers in the saturation regime," *IEEE Photonics Technol. Lett.* **4**(7), 711–714 (1992).
42. A. Yeniay and R. Gao, "Single stage high power L-band EDFA with multiple C-band seeds," in *Optical Fiber Communication Conference (OFC 2002)*, Vol. 70 of OSA Trends in Optics and Photonics Series (Optical Society of America, Washington, D.C., 2002).
43. E. Yahel and A. Hardy, "Amplified spontaneous emission in high-power, Er³⁺-Yb³⁺ codoped fiber amplifiers for wavelength-division-multiplexing applications," *J. Opt. Soc. Am. B* **20**(6), 1198–1203 (2003).
44. G. Meltz, W. W. Morey, and W. H. Glenn, "Formation of Bragg gratings in optical fibers by a transverse holographic method," *Opt. Lett.* **14**(15), 823–825 (1989).
45. O. Humbach, H. Fabian, U. Grzesik, U. Haken, and W. Heitmann, "Analysis of OH absorption bands in synthetic silica," *J. Non-Cryst. Solids* **203**, 19–26 (1996).

1. Introduction

Laser sources locating at eye-safe 2 μm region, especially for operation wavelengths in the atmospheric transmission window between 2.05 μm and 2.3 μm , have many significant applications in atmospheric lidar measurement [1], remote sensing [2], medical surgery [3–5], etc. Compared to conventional solid state lasers, fiber lasers have advantages of high operation efficiency, excellent heat-dissipating capability, good beam quality and compact structure. Currently, the most common fiber laser technology for realizing emission beyond 2 μm is based on the direct energy level transitions ${}^3\text{F}_4 \rightarrow {}^3\text{H}_6$ from Tm^{3+} doped fibers and ${}^5\text{I}_7 \rightarrow {}^5\text{I}_8$ from Ho^{3+} doped fibers. A number of Tm^{3+} -doped, Ho^{3+} -doped and $\text{Tm}^{3+}/\text{Ho}^{3+}$ -codoped silica and fluoride fiber lasers have been reported [6–11].

For Tm^{3+} -doped silica fiber lasers, the reports of an amplified spontaneous emission (ASE) source with a ~ 230 nm spectrum coverage spanning from ~ 1900 nm to ~ 2130 nm [12], a broadband ASE fiber source delivering a ~ 450 nm spectrum covering from ~ 1650 nm to ~ 2100 nm [13] and a superfluorescent source emitting from 1930 nm to 2100 nm with a 170 nm spectrum coverage [14] have demonstrated their potential lasing capability beyond 2 μm region. By using an external diffraction grating, Clarkson *et al* demonstrated a tunable Tm^{3+} -doped silica fiber laser, pumped by 787 nm diode bars, operating at a wide spectrum from ~ 1860 nm to ~ 2090 nm but with a very low efficiency of less than 3% at 2090 nm [15]. Similarly, Guo *et al* reported a tunable Tm^{3+} -doped silica fiber laser, pumped by two 791 nm diodes, with the extended wavelength to ~ 2109 nm and maximum power of approximately 10 W [16]. By using a fiberized grating-based tunable filter, Li *et al* reported a tunable Tm^{3+} -doped fiber laser, core pumped by 1550 nm diodes, operating at a wide spectrum from 1820 nm to 2075 nm with a maximum power of 30 mW and slope efficiency of 27% at 1930 nm [17]. Tokurakawa *et al* demonstrated an ultra broadband wavelength swept Tm^{3+} -doped fiber laser operating from 1750 nm to 2080 nm by using two diffraction gratings and a rotating polygon mirror [18]. Sacks *et al* employed a diffraction grating to demonstrate a tunable Tm^{3+} -doped double clad silica fiber laser, also pumped by two 790 nm diodes, with the reported longest edge at ~ 2188 nm from Tm^{3+} -doped silica fiber laser, however, the slope efficiency at 2188 nm was less than 6% [19].

For $\text{Tm}^{3+}/\text{Ho}^{3+}$ -codoped or Ho^{3+} -doped silica fiber lasers, S. D. Jackson *et al* employed a $\text{Tm}^{3+}/\text{Ho}^{3+}$ -codoped silica fiber to demonstrate a 793 nm diode pumped high power fiber laser operating at wavelength near 2105 nm with a slope efficiency of 42% [8]. Then they demonstrated an 1150 nm diode pumped high-power Ho^{3+} -doped silica fiber laser with the emission wavelength extended to 2120 nm at a slope efficiency of 51% [20]. Hemming *et al* reported a 790 nm diode pumped tunable $\text{Tm}^{3+}/\text{Ho}^{3+}$ -codoped aluminosilicate fiber laser by using a diffraction grating, which achieved a wide spectrum operation from ~ 1850 nm to ~ 2150 nm with a maximum slope efficiency of 25% at 2040 nm [21]. Similarly, Simakov *et al* demonstrated a 1950 nm Tm^{3+} -doped fiber laser pumped tunable Ho^{3+} -doped silica fiber laser operating from 2043 to 2171 nm at an average power of >15 W [22]. Antipov *et al* demonstrated a 1125 nm Yb^{3+} -doped fiber laser pumped Ho^{3+} -doped silica fiber laser emitting at the longest reported wavelength of 2.21 μm from silica-based fiber, however, the maximum output power and slope efficiency were only 130 mW and $\sim 4\%$, respectively [23].

For Tm^{3+} -doped fluoride fiber lasers, ${}^3\text{F}_4 \rightarrow {}^3\text{H}_6$ and ${}^3\text{H}_4 \rightarrow {}^3\text{H}_5$ transitions can operate at 1900 nm and 2300 nm band, respectively [10, 24–27]. Based on ${}^3\text{F}_4 \rightarrow {}^3\text{H}_6$ transition, a 790 nm diode pumped Tm^{3+} -doped ZBLAN fiber laser centered at 1900 nm with a slope efficiency of 33% has been reported [10]. Based on ${}^3\text{H}_4 \rightarrow {}^3\text{H}_5$ transition, El-Agmy *et al* reported a 1064 nm Nd:YAG laser pumped Tm^{3+} -doped ZBLAN fiber laser centered around 2300 nm but with only a maximum power of 150 mW and a slope efficiency of 7.8% due to the transition self-terminating and excited state absorption [27]. For $\text{Tm}^{3+}/\text{Ho}^{3+}$ -codoped fluoride fiber lasers, a 806 nm diode pumped $\text{Tm}^{3+}/\text{Ho}^{3+}$ -codoped ZBLAN fiber laser operating at 2056 nm with a slope efficiency of 36% was demonstrated [9]. For Ho^{3+} -doped fluoride fiber lasers, 1150 nm or 2 μm band lasers are required to be the pump source. Sumiyoshi *et al* demonstrated a Ho^{3+} -doped ZBLAN fiber laser operating at 2 μm pumped by

a 1150 nm Raman fiber laser with a slope efficiency of 33% [28]. Jackson *et al* reported a Ho^{3+} -doped fiber laser pumped by a 2051 nm Tm^{3+} -doped silicate glass fiber laser operating at 2080 nm at a slope efficiency of 72% [29]. Recently, we demonstrated a 1940 nm diode pumped Ho^{3+} -doped ZBLAN fiber laser operating at 2080 nm with a slope efficiency of 78% and a maximum output power 516 mW [11].

Compared to Ho^{3+} -doped fiber, the availability of commercial high power pump diode at 793 nm and the positive “two for one” cross relaxation process between Tm^{3+} ions enable efficiently laser generation from the Tm^{3+} -doped fiber. On the other hand, the fabrication of fluoride fiber is not mature currently and also there are lack of commercial fluoride fiber based components. Therefore, silica fiber based Tm^{3+} -doped lasers are the current best candidate to achieve laser beyond 2 μm with all-fiber structure.

Additionally, multi-wavelength switchable fiber lasers are also desirable because of their applications in photonics true time delay beamforming [30], Dense Wavelength Division Multiplexing (DWDM) [31], fiber sensors [32], etc. The multi-wavelength switchable fiber lasers operating at 1 μm and 1.55 μm bands have been extensively investigated [33–36]. In 2 μm band, only one switchable dual-wavelength Tm^{3+} -doped laser operating at either ~1941.52 nm or ~1942.33 nm was demonstrated recently by employing two high-birefringence FBGs [37].

In this paper, we report the demonstration of a broadband Tm^{3+} -doped silica fiber ASE source with up to ~520 nm spanning from ~1700 nm to ~2220 nm. Based on the ultra-broad ASE spectrum, an all-fiber Tm^{3+} -doped laser was built utilizing either an HR FBG-Fiber end based cavity or an HR FBG-LR FBG based cavity. For this laser, the wavelength selectable range for lasing, the relative thresholds, efficiencies and line width of the laser were investigated. Finally, a six wavelengths switchable laser from 1925 nm and 2200 nm was achieved by employing an FBG array in the cavity.

2. Experiment setup and results

2.1 ASE source

The schematic diagrams of the all-fiber backward and forward ASE sources are shown in Figs. 1(a) and 1(b), respectively. The active fiber used is a double-clad Tm^{3+} -doped fiber (Nufern, SM-TDF-10P/130-HE) with an octagonal shaped pump core with a diameter of 130 μm across the circular cross-section and a numerical aperture (NA) of 0.46. The fiber has a 10- μm core diameter with a reduced NA of 0.15 by a specific pedestal around the core. The Tm^{3+} dopant concentration in the fiber core is about 5 wt. % and the measured absorption coefficient at 793 nm is ~3.0 dB/m. In general, the fiber length is chosen for efficient pump absorption of 15 dB to 20 dB, and thus the length from 5.0 m to 7.0 m should be sufficiently long. However, it has been proved that laser wavelength red-shifts with increasing fiber length induced by re-absorption process at 1.064 μm [38], 1.55 μm [39] and 2.9 μm [28] bands. In order to achieve lasing at longer wavelength, 11.0 m long Tm^{3+} -doped fiber was chosen to strength the re-absorption. Two 793 nm diode lasers (Lumics, German) with 105/125 μm core and cladding parameter multimode fiber pigtail were used as the pump source and the light was coupled into the double-clad Tm^{3+} -doped fiber through a $(2 + 1) \times 1$ pump combiner (ITF, USA). The maximum launched pump power was 8 W. In order to suppress laser oscillation at high power level, one fiber end was angle-cleaved at ~8° to achieve very low feedback while the other fiber end was also angle cleaved at ~5° by using LDC-400 cleaver (Vytran, Germany) instead of 0° to further increase the laser threshold owing to its low reflectivity of ~0.18%. Under this condition, the single-end output for backward ASE or forward ASE can still be realized as a result of the much higher reflectivity from ~5° angle cleaved fiber end compared to that from ~8° angle cleaved fiber end [13]. At the output side, a Germanium window was employed to remove the residual pump light.

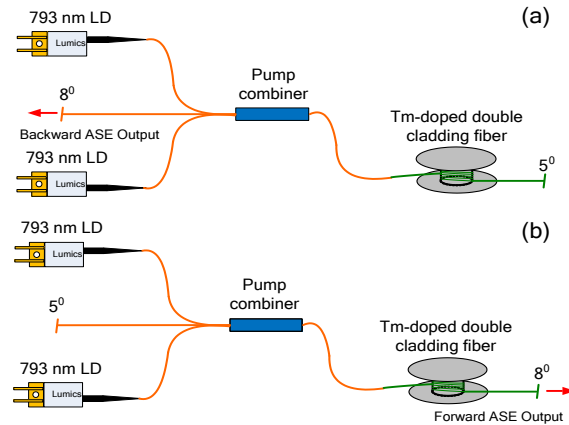


Fig. 1. Experimental setup of the all-fiber Tm^{3+} -doped ASE sources based on (a) backward and (b) forward output.

Figure 2(a) shows the backward and forward ASE spectra measured using an optical spectrum analyzer (Yokogawa AQ 6375) at the launched pump power of 2 W, 4 W, 6 W and 8 W, respectively, and the measured emission and absorption cross-sections between 1700 nm and 2100 nm extracted from Ref. [19] were also given. It is observed that the apophysis region of both backward and forward ASE envelopes increased with raised pump power, but the peak remained essentially unchanged at the regime around 2000 nm. The sharp fall of ASE envelope towards the short wavelength direction can be attributed to the strengthened ground state re-absorption induced by the increased absorption cross-section at shorter wavelength range. The similar fall of ASE envelopes towards the long wavelength direction was observed as well, resulting from the reduced emission cross-section and increased background loss with increasing wavelength. On the other hand, the optical spectrum without a spike at high launched pump power of 8 W suggests that the laser operation mode was successfully suppressed with efficient angle cleaving at the fiber end. The backward ASE spectrum of over 520 nm span from ~ 1700 nm to ~ 2220 nm with a FWHM bandwidth of ~ 60 nm was achieved at the maximum launched pump power of 8 W, which is the reported longest wavelength edge from the ASE of Tm^{3+} -doped fibers. Note that there were noticeable increases in the ASE spectra around 1650 nm, which were clarified as ghost spectra induced by stray light of monochromator usually occurring at the shorter wavelength side of 400 nm away from the original spectra in the spectrum analyser AQ6375 (this has been confirmed by Yokogawa). The stray light has no impact on the original signal and can be ignored. Besides, absorption lines caused by water vapor in the wavelength range from ~ 1800 nm to ~ 1950 nm could be clearly seen in the spectrum. Compared to the backward ASE, the forward ASE had a similar long wavelength edge of ~ 2200 nm but exhibited a narrower spectrum range spanning from ~ 1945 nm to ~ 2220 nm with a FWHM of ~ 35 nm at the launched pump power of 8 W as a result of its stronger re-absorption at un-pumping end [40, 41]. The red-shifted of long wavelength edge in our work can be ascribed to the comparatively long active fiber (~ 11 m) and large rare earth ions concentration (~ 5 wt. %). Larger Tm^{3+} concentration may enable more ground state ions to be involved in the re-absorption process per unit length, and thus stronger total re-absorption can be achieved by using longer fiber. As shown in Fig. 2(b), the populations on the ground manifold were excited to the comparative high Stark levels of laser upper manifold corresponding to the different energy positions by re-absorption of comparative short-wavelength laser. These excited populations were then released to the lower Stark level in a short time via thermal phonon interactions induced energy loss. Originating from the lower Stark level of the upper manifold, longer wavelength emission will be generated. Then the long wavelength emission will act as pump source for the next re-absorption process to produce longer wavelength. Figure 2(c) shows the output powers of

backward and forward ASE as a function of launched pump power. It is observed that their slope efficiencies were both significant low when the launched pump power was below 4 W and then increased quickly with increasing pump power. Maximum output power of 555 mW and 396 mW were achieved at slope efficiencies of 19.4% and 15.8% in the pump power range from 5.5 W to 8 W for the backward and forward ASE, respectively. The output powers from the perpendicular end for both backward and forward ASE were measured to be below 5.0 mW at maximum launched pump power of 8 W indicating the system was essentially operated at single-end output. The better performance of backward ASE compared to forward ASE has been also verified in another quasi-three-level systems [42, 43]. Therefore, the backward ASE was chosen as the broad band source for in situ monitoring of the FBGs in the fabrication. In order to investigate the influence of fiber length on the ASE spectrum, we also measured the backward ASE spectrum using shorter fiber lengths of 5.0 m and 8.0 m and longer fiber of 13.0 m in the system, respectively at the maximum launched pump power of 8 W, as show in Fig. 2(d). Compared to the system using 11.0 m fiber, the shorted fiber system exhibited shorter center wavelength and slight narrower FWHM bandwidth for both backward and forward ASE. For the system using 5.0 m fiber, the center wavelength blue shifted by 13.2 nm and 23.8 nm for the backward and forward ASE, respectively. However, the ASE center wavelength and FWHM bandwidth of the system using 13.0 m fiber were almost unchanged compared to the system using 11.0 m fiber. This suggests that the fiber length of 11.0 m was enough to realize the ASE with the longest edge around 2.2 μm region.

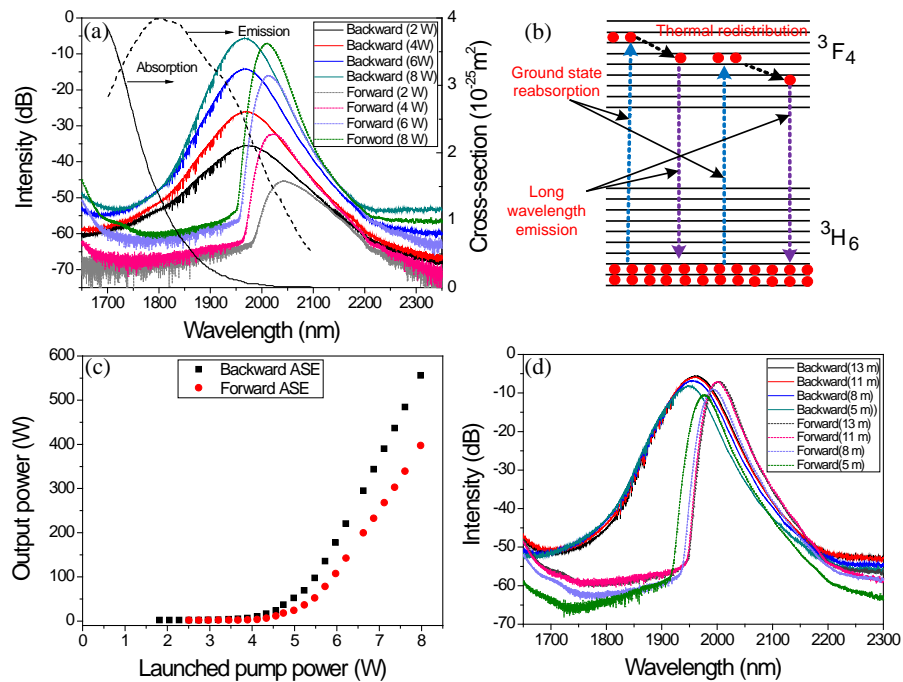


Fig. 2. (a) Measured backward and forward ASE emission spectra at different launched pump powers, and the absorption and emission cross-sections of Tm^{3+} -doped fiber extracted from Ref. [19] are also given; (b) Energy-level re-absorption process of Tm^{3+} -doped fiber laser; (c) Output powers of backward and forward ASE as a function of launched pump power; (d) Backward ASE spectra at different fiber lengths of 13.0 m, 11.0 m, 8.0 m and 5.0 m under launched pump power of 8 W.

2.2 Fabrication of FBGs

All FBGs used in the Tm^{3+} -doped fiber laser system have been fabricated by a 244 nm UV source from a frequency doubled Ar^+ laser using the two-beam holographic technique [44].

The two-beam holographic technique for writing grating structure from the side of fiber is a flexible technique allowing inscribing FBGs with arbitrary wavelengths ranging from 750 nm to 2300 nm in our laboratory. For mid-IR fiber laser applications, we have UV-inscribed FBGs with centered wavelengths in the range from 1800 nm to 2225 nm, which coincides with the ASE wavelength range of Tm^{3+} -doped fiber. The ASE generated from Tm^{3+} -doped fiber was also employed as a broadband light source for in situ monitoring of the FBGs in the fabrication.

We have attempted to UV-inscribe FBGs on Corning SM28 and Thorlabs SM2000 fibers to compare their characteristics. Note, before the FBG inscription, the SM28 and SM2000 fibers were hydrogen loaded under high-temperature (80°C) and high-pressure (150 bar) for 2 days to increase their UV-photosensitivity. However, a great quantity of hydroxide ions that were contained in hydrogen loaded fiber strongly absorbing the light in the wavelength range from 1800 nm to 1900 nm and beyond 2200 nm [45]. Therefore, the spectra of FBGs with Bragg resonances in these two wavelength ranges were not be possibly monitored in the fabrication and were measured after the annealing treatment, which out-gas the hydrogen from the fiber. All FBGs have been annealed at 80 °C for 48 hours to improve their long term stability. Figure 3 shows the measured transmission spectra of six FBGs inscribed on the SM28 and SM2000 fibers centered at ~1800 nm, ~2050 nm and ~2225 nm, respectively. From Fig. 3 we can see that after annealing, the transmission loss peaks of the six FBGs reached around 16-20 dB, corresponding to a reflectivity of 96-99%; the 3 dB bandwidths (FWHMs) were all less than 0.4 nm. It also can be observed that the FBGs UV-inscribed in SM28 fiber are stronger with slightly high reflectivity and broad bandwidth in comparison with the FBGs made in SM2000 fiber.

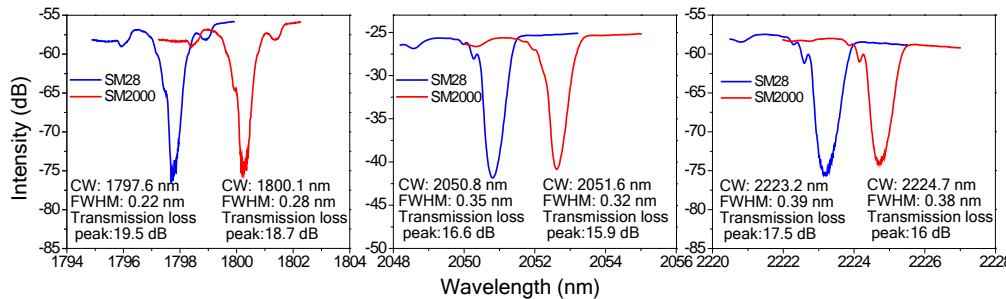


Fig. 3. Measured transmission spectra of the FBGs inscribed in SM28 and SM2000 fibers, respectively.

2.3 Wavelength selectable range based on FBGs

Concerning the large spanning of the ASE towards longer wavelength range that may provide the possibility of laser operation at wavelength beyond 2150 nm, the investigation on wavelength extension range of Tm^{3+} -doped fiber laser has been performed. Figures 4(a) and 4(b) show two Tm^{3+} -doped silica laser systems exploiting low reflectivity (LR) FBG and cleaved fiber end as the output couplers, respectively. In order to compare with previous ASE measurement while identify the lasing wavelength limit beyond 2150 nm, we used 11.0 m Tm^{3+} -doped fiber in this case. At the output end, either the fiber end facet (~3.5% Fresnel reflection) [Fig. 4(a)] or LR FBG [Fig. 4(b)] was employed to provide laser feedback and also act as the output coupler. A number of FBGs were UV-inscribed with the Bragg reflection wavelengths between 1900 nm and 2200 nm at a span of ~25 nm for the investigation. The HR FBG was designed with receptivity of > 95% and a spectral FWHM of <0.4 nm, and the LR FBG was designed with receptivity of ~50% and a spectral FWHM of <0.4 nm. Because the threshold for Fresnel-reflection-based cavity might be lower than that for the FBG-based cavity at some wavelengths of small gain, the fiber end at the FBG side was angle cleaved at 8° to reduce the reflection in order to avoid the parasitic lasing.

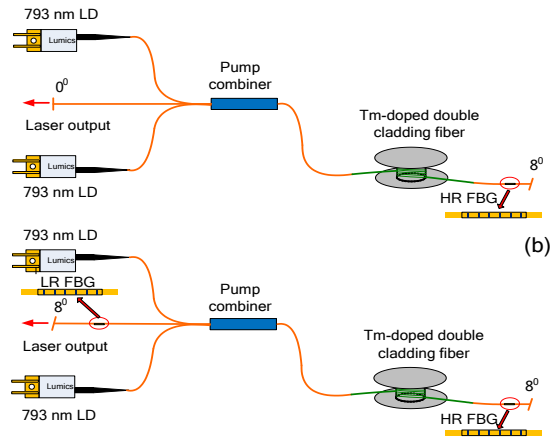


Fig. 4. Experimental setup of Tm^{3+} -doped silica fiber laser with counter-propagating scheme employing (a) $\sim 3.5\%$ reflectivity of cleaved fiber end and (b) $\sim 50\%$ low reflective (LR) FBG as output coupling reflectors.

By using the setup shown in Fig. 4(a), the narrow width CW laser with selectable wavelength between 1975 nm and 2150 nm was achieved. Figure 5 shows the spectra of lasers centered at 1974.7 nm, 1997.5 nm, 2026.2 nm, 2056.8 nm, 2074.3 nm, 2102.4 nm, 2125.7 nm and 2151.02 nm at the maximum launched power of 8.0 W measured in a large spectrum range of 400 nm. It is observed that the laser was significantly stronger than ASE, especially at the regions of 2025 nm \sim 2075 nm where the suppression of ASE was more than 60 dB. Though the ASE was strengthened as further deviation of laser wavelength from this region, the ASE suppressions of ~ 42 dB and ~ 35 dB were also achieved at 1974.7 nm and 2150.02 nm, respectively.

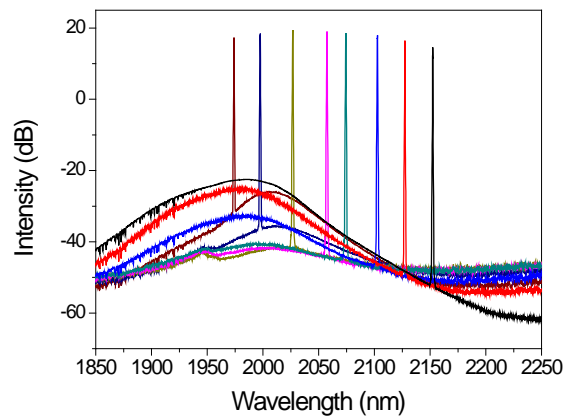


Fig. 5. Output spectra of Tm^{3+} -doped fiber lasers at 400 nm spectrum range for cavity constructed by perpendicular cleaved fiber end and HR FBGs. From left to right these center wavelengths were 1974.7 nm, 1997.5 nm, 2026.2 nm, 2056.8 nm, 2074.3 nm, 2102.4 nm, 2125.7 nm, and 2151.02 nm, respectively. The scanning resolution was 0.5 nm.

The spectra of the lasers were also measured in a 1.0 nm range with a resolution of 0.02 nm to investigate their spectrum characteristics, as shown in Fig. 6. It is observed that the FWHM of laser lines were all narrower than 0.3 nm suggesting the efficient spectral confining ability of the HR FBGs. Note that the spectrum gradually tended to be compressed and smoothed with increasing output wavelength owing to the weakened ground state re-absorption process at longer wavelength region. At the shorter wavelength emission region, especially below ~ 2000 nm, the spectrum was broader and exhibited more amplitude fluctuation as a result of strong ground state re-absorption and re-emission processes. After

the center wavelength exceeding ~ 2100 nm, the spectrum width was essentially unchanged suggesting that the laser was almost not influenced by the re-absorption owing to the fairly low absorption cross-section of less than $0.1 \times 10^{-25} \text{m}^2$. The measured output powers as a function of the launched pump power relevant to different emission wavelengths are shown in Fig. 7. Note that the laser thresholds were accurately measured according to the spectra and the output laser power was calculated by subtracting the ASE power at laser threshold from the total output power. A maximum output power of >2.1 W can be obtained at the range from ~ 1997 nm to ~ 2100 nm with a slope efficiency of $>42\%$. According to the varied thresholds with respect to different emission wavelengths, we can observe that the firstly resonant wavelength here is located at the regime around ~ 2074 nm.

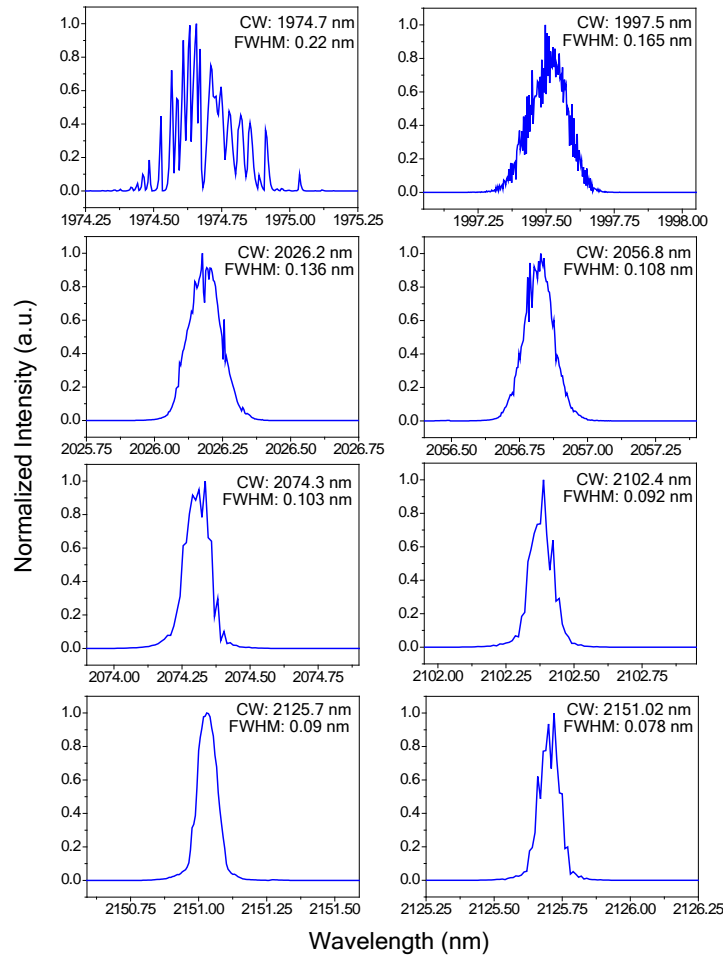


Fig. 6. Output spectra of Tm^{3+} -doped fiber laser for cavity constructed by perpendicularly cleaved fiber end and HR FBGs with different center wavelengths. The scanning range and resolution were 1 nm and 0.02 nm, respectively.

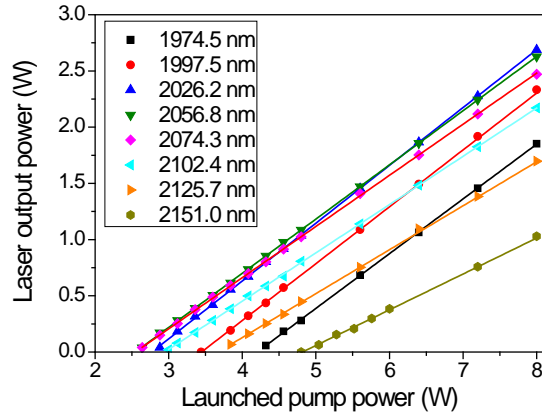


Fig. 7. Output laser power as a function of launched pump power with different center wavelengths of 1974.7 nm, 1997.5 nm, 2026.2 nm, 2056.8 nm, 2074.3 nm, 2102.4 nm, 2125.7 nm, and 2151.02 nm.

In order to investigate the laser wavelength operation limit of our Tm^{3+} -doped silica fiber, higher feedback was added by employing LR FBG to replace the previously cleaved fiber end as the output coupler, as shown in Fig. 4(b). The short and long wavelength edges were then extended to 1925.6 nm and 2198.4 nm respectively. Figure 8 shows the measured spectra across 400 nm spectrum range at the maximum launched power of 8.0 W. Though the fraction of ASE in the output was raised with increased wavelength deviation from the region around 2050 nm, the laser at 1925.6 nm and 2198.4 nm still gave an ASE suppression of ~45 dB and ~33 dB, respectively.

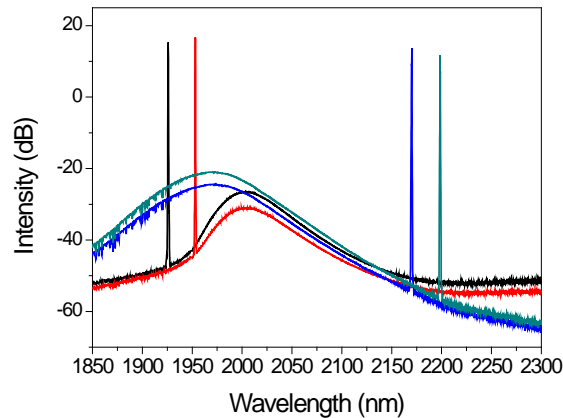


Fig. 8. Output spectra of Tm^{3+} -doped fiber laser at 400 nm spectrum range for cavity constructed by LR FBG and HR FBG. From left to right these center wavelength were 1925.6 nm, 1951.2 nm, 2174.9 nm, and 2198.4, respectively. The scanning resolution was set at 0.5 nm.

The spectra of the lasers under each LR FBG at a narrow scanning range of 1.0 nm were also measured at the maximum launched pump power of 8 W to exhibit the detailed spectrum characteristics as shown in Fig. 9 with center wavelengths of 1925.6 nm, 1951.2 nm, 2174.9 nm and 2198.4 nm, respectively. The operation wavelength of 2198.4 nm is also the longest wavelength produced from ${}^3\text{F}_4 \rightarrow {}^3\text{H}_6$ transition of Tm^{3+} ions so far being demonstrated. Similar to the results as shown in Fig. 6, the laser at 1925.6 nm and 1951.2 nm still exhibited spectrum fluctuation and broadening, whereas the laser at 2174.9 nm and 2198.4 nm showed fixed spectrum width of 0.8 nm and relatively smooth and narrow spectrum. Figure 10 displays the measured output power as a function of the launched pump

power relevant to different emission wavelengths. It is observed that the laser emitting at 2198.4 nm can still operate at a comparatively high slope efficiency of 17.82% with a low threshold of 4.78 W and a maximum output power of 0.55 W, which can be ascribed to the high feedback provided by the pair of FBGs and strengthened re-absorption induced by long active fiber and large ions concentrations.

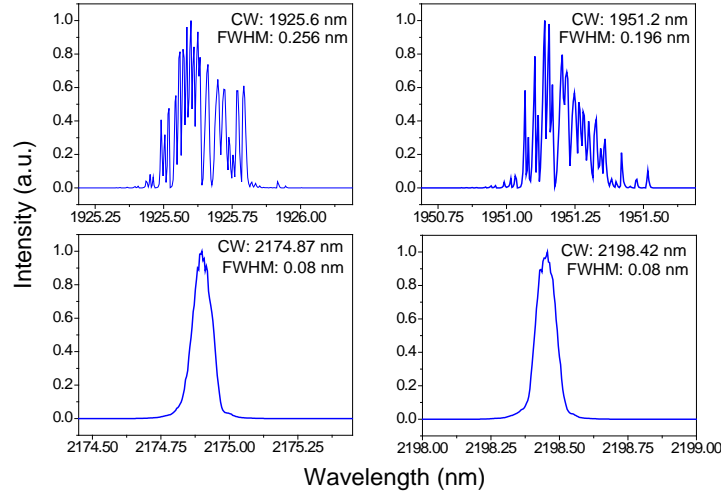


Fig. 9. Output spectra of Tm^{3+} -doped fiber laser for cavity constructed by LR FBGs and HR FBGs with different center wavelengths. The scanning range and resolution were 1 nm and 0.02 nm, respectively.

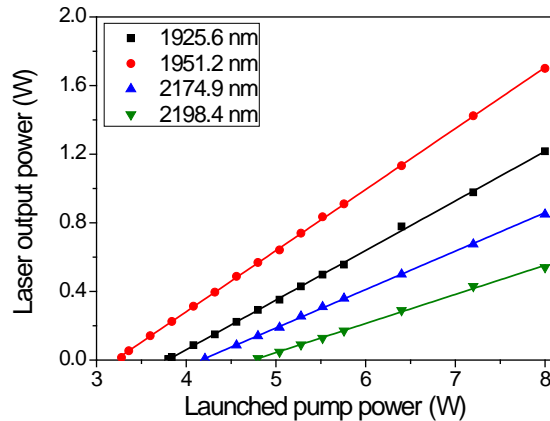


Fig. 10. Output laser power as a function of launched pump power with different center wavelengths of 1925.6 nm, 1951.2 nm, 2174.9 nm and 2198.4 nm.

Figure 11 shows the slope efficiency and threshold as a function of the launched pump power employing either cleaved fiber end or LR FBG as the output coupler. It is observed that the slope efficiency increased to the maximum at the region around 2020 nm and then decreased near linearly with wavelength resulting from the significant decreasing emission cross-section and increasing background loss. The minimum threshold was achieved at the region around 2060 nm where the absorption cross-section was near zero and thus the cavity loss caused by re-absorption is negligible. Note that the threshold at wavelength above ~ 2060 nm increased quickly with wavelength as a result of the weakened gain and increasing background loss. A Stokes efficiency limit given by $\lambda_{\text{pump}}/\lambda_{\text{laser}}$ as a function of laser wavelength was also added to Fig. 8. We can clearly see that the emission modes ranging from ~ 1974.7 nm to ~ 2125.7 nm can be operated at slope efficiencies exceeding the Stokes

limits. A maximum slope efficiency of 51.42% with respect to launched pump power at ~2026.2 nm indicated that at least 31.37% of the Tm^{3+} ions participated in the “two for one” cross relaxation process producing two laser photons when the ground state ion was excited to the upper 3H_4 level. Although the slope efficiency was decreased to 17.82% at 2198.4 nm as a result of fast increasing background loss and decreasing emission cross-section with wavelength, it still exhibited good stability and spectra confining ability.

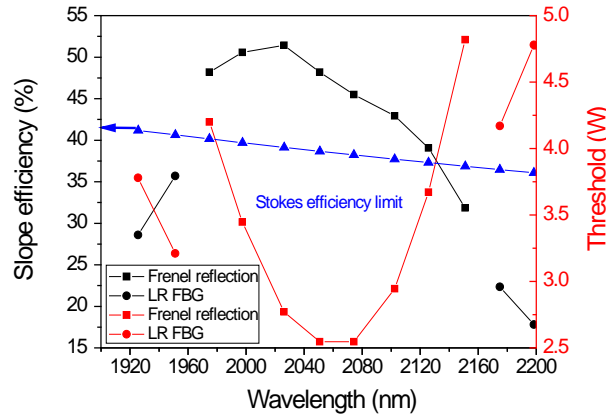


Fig. 11. Dependence of laser slope efficiency and threshold on center wavelength by employing perpendicularly cleaved fiber end and LR FBG as output coupler, respectively.

2.4 Wavelength switchable operation based on an FBG array

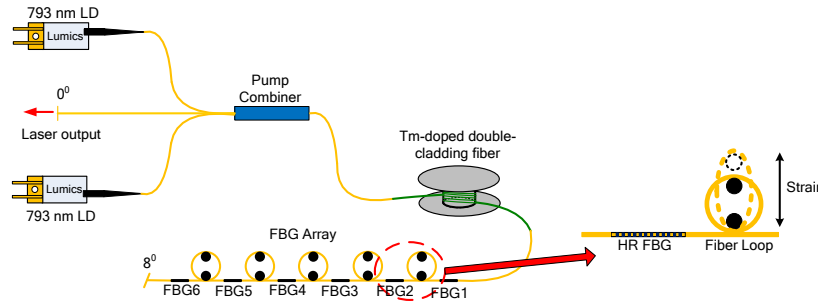


Fig. 12. Experimental setup of multi-wavelength switchable Tm^{3+} -doped silica fiber laser.

It is well known that there are many methods of tuning or switching the wavelength of a fiber laser such as strain tuning an FBG, fiber etalons, external diffraction grating, fiber coupled acousto optic tunable filters and so on, all of which have their own advantages and drawbacks. For strain tuning an FBG, it is of low insertion loss and compact structure, but its tuning range is less than 3 nm in general case. The external diffraction grating can cover a large tuning range but needs a free space structure. The fiber etalons and fiber coupled acousto optic tunable filters are absolutely favourite components to tune the wavelength in a continuous range with higher speed, but their current insertion losses at 2 μm are still comparatively large and there are no such commercial products at 2 μm currently. In our work, we have mainly focused on switching the laser in a large spectrum range based on our in-house fabricated FBGs. An FBGs array with different centre wavelengths were employed to demonstrate a large switchable wavelength range in our Tm^{3+} -doped fibre laser although it was not continuous switching. This method can cover larger switching range while maintain the advantage of all-fibre structure and low insertion loss. The experimental setup of a multi-wavelength switchable Tm^{3+} -doped fiber laser is shown in Fig. 12. The signal input end of the

pump combiner was perpendicularly cleaved to provide Fresnel reflection for all wavelengths while acting as the output coupler. Its output end was spliced to 11 m Tm^{3+} -doped double-clad fiber, as the same configuration shown in Fig. 4. The other end of the Tm^{3+} -doped fiber was spliced to a specifically designed FBG array consisting of six HR FBGs. According to the measured thresholds in section 2.3, we fabricated these FBGs with center wavelengths as the order of decreasing thresholds, i.e., FBG1 (~1997 nm), FBG2 (~2125 nm), FBG3 (~2025 nm), FBG4 (~2103 nm), FBG5 (~2075 nm) and FBG6 (~2057 nm), of which the FBG array transmission spectrum is shown in Fig. 13(a). The pigtailed between adjacent FBGs in the array were looped around two tubular mounts at a radius of 5 cm. With this setup, the wavelength can be switched freely by increasing the distance between the two tubular mounts after the selected FBG to induce the bend loss for the suppression on all other laser modes relevant to the FBGs after the selected FBG. Through mode competition, the laser mode relevant to the selected FBG can win owing to its lower threshold, of which the measured spectra from output side are shown in Fig. 13(b).

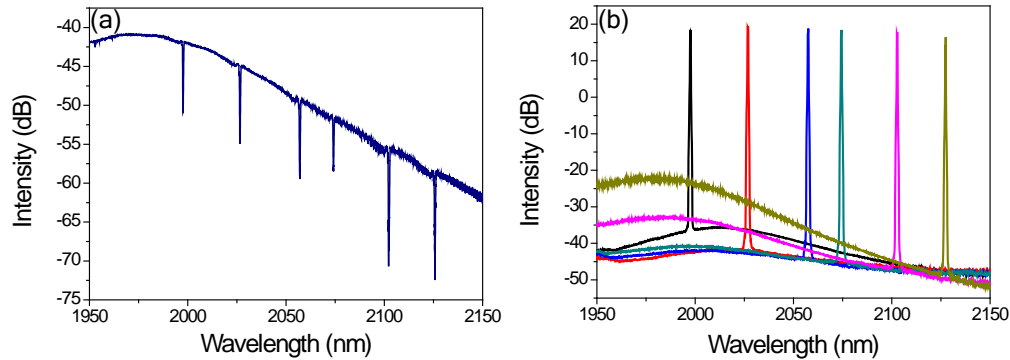


Fig. 13. (a) Transmission spectrum of the FBG array and (b) output spectra of the multi-wavelength switchable Tm^{3+} -doped fiber laser.

4. Conclusion

In this paper, an all-fiber Tm^{3+} -doped fiber laser whose wavelength can be selected from 1925.6 nm to 2198.4 nm by using specifically designed FBGs with different center wavelengths as the cavity HR reflectors and LR output couplers. The wavelength of 2198.4 nm is also the longest wavelength so far reported from the Tm^{3+} -doped fiber laser based on the ${}^3\text{F}_4 \rightarrow {}^3\text{H}_6$ transition. Additionally, a six wavelengths switchable Tm^{3+} -doped fiber laser based on an FBG array has been presented. It can be concluded that long fiber length and large ions concentration have benefited wavelength extension of both ASE and laser spectrum in Tm^{3+} -doped fiber lasers. However, further large-scale extending of wavelength through this method might be difficult due to the limitation of the intrinsic maximum energy difference between ${}^3\text{F}_4$ and ${}^3\text{H}_6$ and the significantly increased background loss beyond 2.2 μm in silica fiber. Efficient laser generation from 2.2 μm to 2.6 μm could be achieved by considering new dopant ions or cascade Raman laser based on low phonon energy materials such as fluoride-, chalcogenide- and telluride-based fibers.

Acknowledgments

This work was supported by National Nature Science Foundation of China (Grant No. 61377042 and 61107037), and European Commission's Marie Curie International Incoming Fellowship (Grant No. 911333). The work was also partly supported by Science and Technology Innovation Team of Sichuan Province (No. 2011JTD0001).